The Heat Flux Method adapted for hybrid iron-methane-air flames

The Heat Flux Method adapted for hybrid iron-methane-air flames

M.R. Hulsbos*[1], R.T.E. Hermanns[1], R.J.M. Bastiaans[1], and L.P.H. de Goey[1]

[1]Eindhoven University of Technology, Power & Flow Group, Department of Mechanical Engineering, Building 15, Gemini-south, Groene Loper, P.O. Box 513, 5600 MB Eindhoven, the Netherlands

Abstract

Recently a cyclic energy storage concept was proposed in which metal powders are used as CO_2-free energy carrier: the metal fuel cycle. In this cycle, the burning of iron powder is considered as the discharge of the energy carrier. However, for this cycle to be a efficient one, more understanding of the laminar burning velocity of iron powder is needed. Therefore, a new burner - based on the Heat Flux Method (HFM) - is proposed which can measure the burning velocities of flat hybrid iron-methane-air flames. In this paper, this burner is described and a proof of burner is given by first results. They show a decrease in burning velocity when iron is added to a stoichiometric methane-flame. Further analysis of these results show that the opportunities for improvement lay in limiting the fluctuations for iron-concentrations in the flame on small time scales.

Keywords: Metal Fuels, Iron Combustion, Burning Velocity, Heat Flux Method, Laminar Flames

1 Introduction

Nowadays, it is evident that the current CO_2 emissions have a large negative impact on the environment. According to the World Energy Outlook of the International Energy Agency (IEA), current emission policies (2021) will cause the global temperature to keep rising till 2100 with a total increase of 2.6 °C [1]. However, in a scenario where the world goes to a net-zero-emission (NZE) society in 2050, the temperature rise can be limited to 1.5 °C. But to meet this goal, technological development is needed to cope with issues in the energy transition.

It is expected that a large part of the energy sector will be electrified and supplied mainly by clean energy from wind and solar, which is well known for its intermittency. Demand for energy storage is thus expected to increase. Batteries will take up the biggest share of this storage with an increase of 18 to 30 times of its capacity this decade [1, 2]. This however, will put pressure on the lithium, nickel and cobalt demands, and also leave the issues for heavy duty long range transport sectors unresolved. The lithium price for example, has increased 500% in 2021 due to its high demand [3]. It can thus be stated that different energy storage technologies are needed to meet the NZE goals.

Hydrogen and ammonia can be part of the solution. However, issues with safety, density and long term storage have not yet been fully tackled [4–6].

Metal fuel cycle Recently, a concept of using metal powders for the storage of clean energy has been proposed [4, 7]. In this concept clean energy can be stored in iron powder by reducing iron oxides. This clean energy can then be safely packed and transported. When needed, the iron powder can be burned using direct combustion: $Fe + O_2 \longrightarrow Fe_2O_3$. Since there is no carbon present in iron, no CO_2 is emitted in the combustion process and the only product is iron oxide powder. By capturing the particles after combustion, and reduce them back into iron with clean energy, the metal fuel cycle becomes a closed system. The whole metal fuel cycle is illustrated in figure 1. To kick-start this novel technology, better understanding of the processes involved in this cycle is needed. In this paper it is shown that the the burning velocities of iron aerosols can be measured by using the Heat Flux Method (HFM) [8] with the aid of methane as a stabilizing agent. The effect of iron powder on the burning velocity of methane can be addressed when added to a methane flame. Since the properties of CH_4 are well know, and the flow profile is relatively simple, results from such hybrid flames with methane and iron are particularly suitable for comparison with simulations. The experimental results are obtained by adapting of the Heat Flux Burner (HFB)[8] for hybrid flames.

Laminar burning velocities Earlier results on the topic of burning velocities of iron flames are not easily comparable since the powders and experimental equipment vary widely. Sun et al [9, 10] found that particles with a D_{50} of $\sim 3\mu m$ have a burning velocity that ranges from 10 to 35 cm/s in a spherically expanding flame. Here, a dependence of the burning velocity on the equivalence ratio was found, with a maximum burning velocity at stoichiometric conditions.

Tang et al. [11, 12] conducted micro-gravity experiments with particles suspended in air, and oxygen argon mixtures. Their results indicated that the burning velocity of iron combustion in air heavily relies on the (mean) particle size, in which the burning velocity is inversely proportional to the particle size. In addition to these micro-gravity experiments, McRea et al. [13] re-

*Corresponding author: m.r.hulsbos@tue.nl

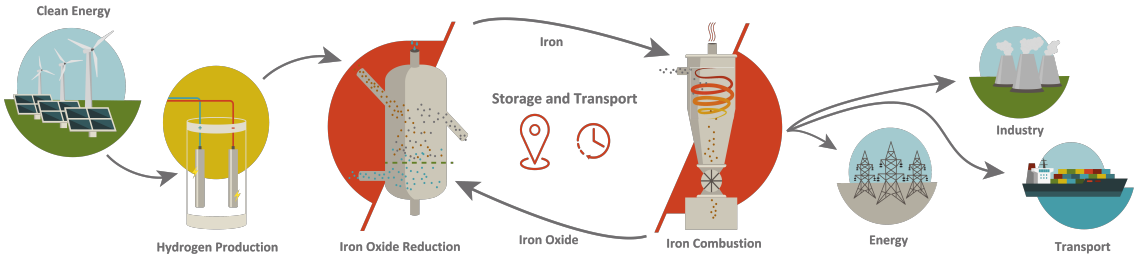

Figure 1: The metal fuel cycle.

produced the burning velocity results form Tang [11, 12] for oxygen argon mixtures in a counterflow burner with reasonable accuracy. Simulations of Wen et al. [14] could reproduce the results from the counterflow burner globally.

Recent measurements with a tube burner by Fedoryk et al. [15] show that the burning velocity of iron in air ranges from 10 to 18 cm/s when particles with a D_{50} of ~ 13 µm are used and that the burning velocity - in contrary to Sun et al. [9, 10] - is not sensitive to the equivalence ratio of the flame.

Hybrid iron-methane-air flames - like in this paper - where investigated by Julien et al. [16]. They added iron particles with a Sauter mean diameter $D_{32} = 2.2$ µm, to a stoichiometric methane flame in a modified Bunsen burner. A decline in burning velocity from ~ 35 cm/s to ~ 15 cm/s was observed in the range of 0 to 250 g/m^3 iron loading. This study was used as main comparison material in this paper.

The Heat Flux Method The HFM was developed in the late 20th century by de Goey and van Maaren [17], inspired by the concept of Botha and Spalding [18], and later investigated, developed and used in research concerning laminar burning velocities [8, 19–24]. In accordance with this method the Heat Flux Burner (HFB) was developed. The method is based on creating gaseous flames on a perforated plate. The rim of the plate is kept at constant temperature by hot water at around 95 °C. Since the flame can be assumed flat [19, 21, 23], the temperature of the burner plate as a function of the radius can be used as a way to measure the heat loss of the flame to the burner plate. Since the burner plate is heated by both the water at the rim and the flame, it's temperature is elevated above the unburned gas temperature, thus allowing for preheating of the gas mixture by the burner plate. There are thus 3 heat fluxes in the burner as illustrated in figure 2. 1. From the flame to the burner plate. 2. From the burner plate to the unburned mixture, and 3. From the burner plate to the hot water or vice versa. This last heat flux can be calculated by measuring the temperature gradient over the burner plate in radial direction. In the HFM, this is done by attached thermocouples at the bottom of the burnerplate. For a more extended review of the HFM, one is referred to Alekseev et al. [25].

Heat fluxes:
1. from flame to burnerpalte
2. from burnerplate to unburned gas
3. from or to the hot water

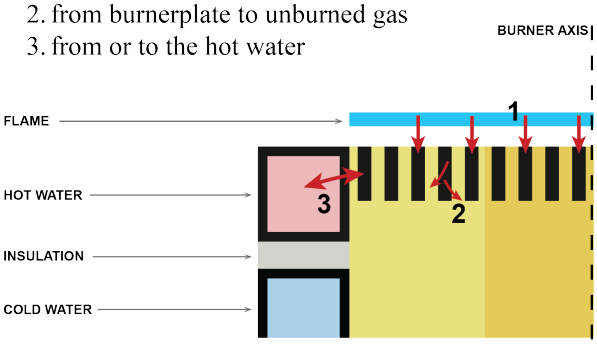

Figure 2: Schematic explanation of the heat fluxes involved in the heat flux method.

2 The Heat Flux Burner for hybrid flames

For hybrid flames, i.e. gaseous flames with solid particles, this HFM could operate in the same way as mentioned in the previous section. However, since the mixture now consists of both a solid as a gaseous fuel, the properties of the flow change significantly. Therefore, adaptions to the classical HFB are necessary in order to create a HFB suitable for hybrid flames: a Hybrid Heat Flux Burner (HHFB). These adaptations can be summarized in 2 parts. The adaptation of the mixing chamber upstream from the burner plate, and the addition of a dispersion system for the generation of a stable flow of iron particles mixed with methane-air. An overview of the setup is described in the next paragraph.

Setup overview The setup is based on the heat flux burner setup as described by Bosschaart and de Goey [22] and is schematically illustrated in figure 3. In this setup, the flow of gaseous substances is controlled by Brockhorst Mass Flow Controllers (MFCs). Downstream of the MFCs, the methane and air flows are combined and send through a 25°C water basin via a copper coil to assure a correct unburned gas temperature T_u. The coil is connected via a dispersion system to the

burner. The burner consists of 2 parts which are separated by thermal insulation. A cold bottom part - cooled by the 25°C water basin - and a hot top part, consisting of a heated ring around the perforated plate. The rim is kept at 95°C using a water basin. Type-T thermocouples are used to ensure the measurement of the temperature of the cold water basin and the burner rim. 15 Type-E thermocouples are used to monitor the radial temperature profile of the burner plate. The dispersion system, MFCs, and thermocouples are connected by a NI DAQ to a lab PC. LabVIEW is used to control the MFCs and dispersion system while also reading the thermocouples and iron mass flow. Downstream of the burner, a Nilfisk VHS110 ATEX cleaner with a bag filter and HEPA filters is used to collect the burned particles.

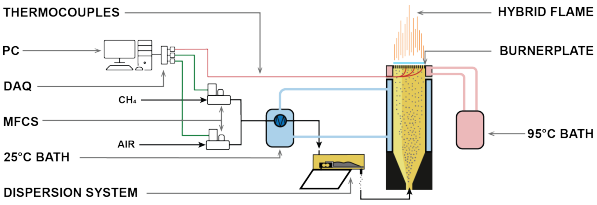

Figure 3: Overview of the setup with HHFB and corresponding infrastructure.

Dispersion system For a continuous flow of iron to the burner, a dispersion system was developed based on a vibrating conveyor principle. A hopper and gutter are mounted on a Tuxel electromagnetic feeder LEV-4. The electromagnetic feeder is controlled using a thyristor which allows for the management of the amplitude of the vibrations send to the hopper and gutter.

In addition to the hopper and gutter, a loadcell is mounted inbetween the electromagnetic feeder and hopper/gutter. The system is schematically displayed in figure 4. This way, the mass flow from the hopper to the burner can be logged. The chosen method contrasts with dispersion systems form Goroshin et al. [26] and Julien et. al. [27] which combine a piston dispersion system with Laser Attenuation (LA). The main advantage of a loadcell based system over a LA based dispersion system is that there is no need for calibration of the mass flow. The chosen loadcell is the KERN CP10-3P1 with a nominal load of 10 kg and full scale error of 0.023%. The typical mass loaded on the loadcell is in the order of 200 g. Meaning that during experiments, the loadcell only had to suffer weights in the range of $\sim 2\%$ of the max load. Due to the over-dimensionalization of the loadcell, the system was rigid enough to overcome the vibrations and still give accurate results. Over the hopper, gutter and loadcell, a lid is placed with an input for gas flow. This way, the dispersion system is incorporated as a closed system upstream of the burner.

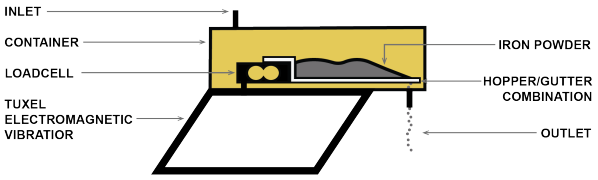

Figure 4: Schematic overview of the dispersion system used.

Particles and dynamics A limitation in creating a HHFB for iron particles is the relatively large terminal velocity compared to the burning velocity of iron aerosols [9, 11, 12, 15]. Where in the Bunsen-type burners, the gas velocity exceeds the burning velocity of a mixture, the goal of the HFM is to match the burning velocity to the gas velocity of the mixture closely. The iron powder used in these experiments is Sigma Aldrich carbonyl powder (product number 44890). This powder has a D_{50} of ~ 7 µm and a D_{90} of ~ 14.5 µm by mass, determined by using laser diffraction of the Bettersizer S3 Plus. The particle size distribution by mass is shown in figure 5.

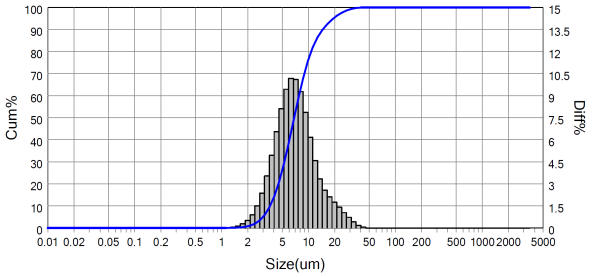

Figure 5: Particle Size Distribution (PSD) by mass of the Sigma Aldrich carbonyl (SA) powder used in the experiments. Measurements were done using the Bettersizer S3 Plus.

This powder was chosen to due to its relatively low terminal velocity, illustrated in figure 6. From the literature overview it can be assumed that the chosen iron particles will have a burning velocity well above 10 cm/s [9, 11, 12, 15]. Comparing these results for the burning velocity with the terminal velocity of the SA powder, it can be concluded that all but a negligible part of the particles will be able to be carried up by the unburned gas to the flame provided the geometry of the burner is well designed.

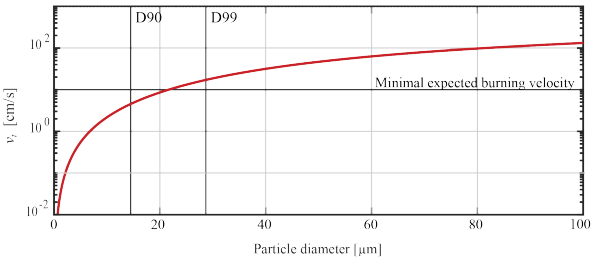

Figure 6: Terminal velocity v_t of iron particles in ambient air at STP according to Stokes law.

Hybrid burner geometry The original HFB has a distribution-plate to break up any jet coming into the mixing chamber from a tube or hose, and a wide section to optimize mixing of gasses. This also allows for the ability to create a contraction towards the burner plate, thus ensuring a reasonably flat flow profile for gaseous mixtures [20, 23]. However, the high density of iron accounts for a high terminal velocity compared to the low gas velocities in the wide mixing chamber. This raises the issue of large quantities of iron accumulated in the mixing chamber in the case of a classic heat flux burner. To minimize the accumulation of iron in between the flame and the dispersion system, the mixing chamber was redesigned as illustrated in figure 7. To avoid low velocities and eddies, the mixing chamber was replaced with a diverging cone of 16 degrees, connecting a 4 mm inner diameter hose to a 30 mm diameter pipe.

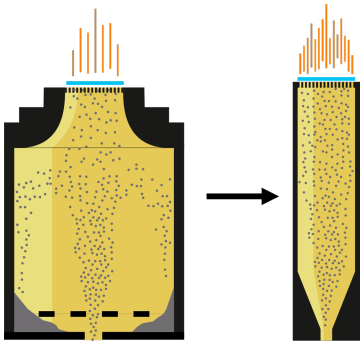

Figure 7: Changes in burner geometry from the classical burner with distribution plate (left) to the simpler hybrid burner (right).

Powder accumulation It was found that after a while, the iron flow at the burner plate would start to fluctuate due to an avalanche effect from particles settled on the inner burner wall. Particles accumulate there slowly until they fall back down into the flow thus creating a burst of iron in the flame. This was also observed by Fedoryk et al. [15]. To minimize this avalanche effect, a DC motor was installed with a small hammer and spring to knock the burner throughout experiments, shaking off the particles from the burner wall continuously. To avoid clogging of the powder in the dispersion system by arching or bridging effects, the powder was prepared by drying it in a vacuum oven at 150°C (at least for 12 hours).

3 Results

Methane-air flames As a baseline test for the HHFB, burning velocities of methane flames were measured. In figure 8 the measured temperatures of the burnerplate are shown for different gas velocities. Here, curves show a parabolic fit of the form $T_{fit} = \alpha r^2 + T_0$. The HFM identifies the case where no net heat flux, from or to the burner plate, is present. This is obtained when $\nabla T = 0$, $T_0 = T_{fit}$ and thus $\alpha = 0$. The case for $\alpha = 0$ can be found by linear interpolation of parabolic coefficient α as function of the gas velocity v_g. For example, figure 9 shows the of interpolation to the measured burning velocity of a stoichiometric methane flame to be 35.7 cm/s in the case of the HHFB. These measurements were then done for several different equivalence ratios for methane-air flames.

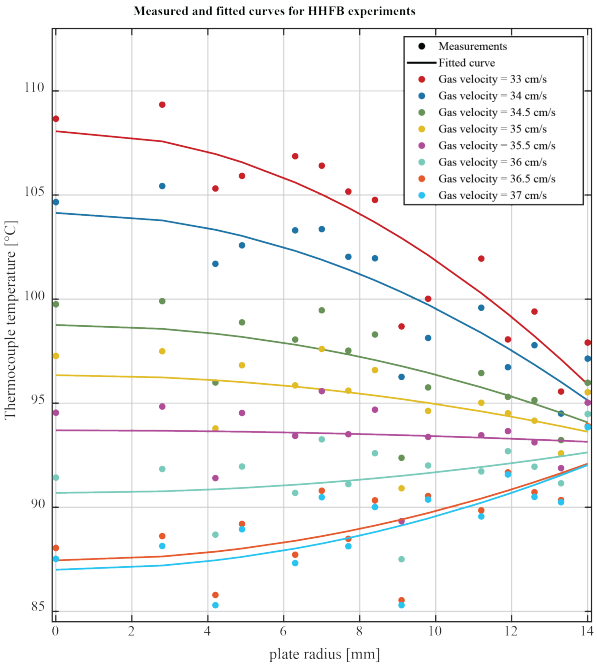

Figure 8: Measurement of the burning velocity of a stiochiometric methane-air flame in the HHFB. The temperature distribution of the burnerplate is given by the thermocouples placed at the bottom of the burnerplate. Dots indicate the average temperature over time for a corresponding gas velocity. Lines indicate the best fit corresponding to the measurements in the shape of $T_{fit} = \alpha r^2 + T_0$.

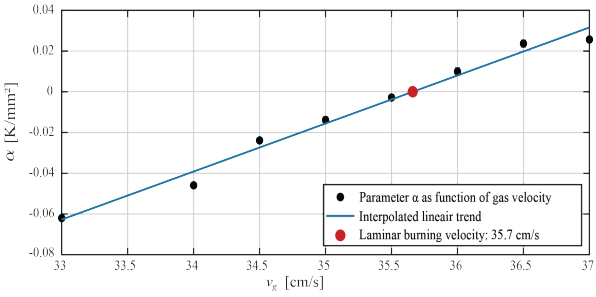

Figure 9: Interpolation of the parabolic coefficient to the adiabatic burning velocity of a stoichiometric methane flame. Each dot indicates a parabolic coefficient α from a fit of figure 8. S_L is indicated in red.

In figure 10 the results of methane flames at different equivalence ratios are compared to results from a HFB using the same infrastructure as the HHFB[1] and results from literature [28]. Good agreement was found

[1] The same software, MFCs, hoses, and cooling and heating mechanisms.

for the $\phi - S_L$ curves of the HFB and HHFB in the current infrastructure while slightly shifted burning velocities were measured compared to the measurements of Hermanns [28].

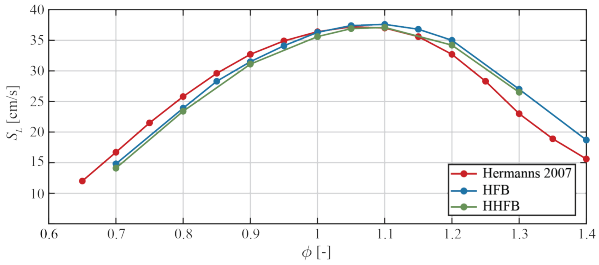

Figure 10: Validation of the HHFB by comparison of methane-air burning velocities as a function of equivalence ratio with the HFB in the current setup and from earlier HFB literature [28].

Hybrid flames For the proof of burner, it is chosen to use a stoichiometric methane-air flame as starting point. Iron was then added to this mixture creating a fuel rich hybrid flame. A picture of such a typical hybrid iron-methane-air flame produced by the HHFB is shown in figure 11b while 11a shows a methane flame.

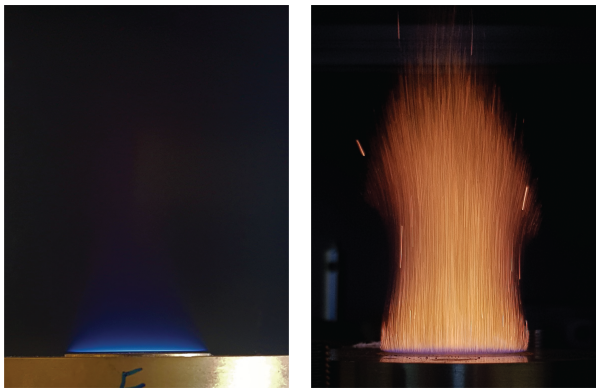

(a) Methane flame produced by the HFB with $\phi_{CH_4} = 1$, $v_g = 36$ cm/s

(b) Typical hybrid flame produced by the HHFB with $\phi_{CH_4} = 1$, $v_g = 35$ cm/s and $C_{Fe} = 22$ g/m^3

Figure 11: Methane (a) and hybrid (b) flames produced by the HHFB.

Results from the HFM used on such hybrid flames are shown in figure 12. This graph is similar to the one shown in figure 9, however, the linear interpolation of α is done as a function of the iron concentration C_{Fe} instead of v_g. This way the concentration of iron needed for a mixture to match its burning velocity to the given gas velocity can be calculated. The found burning velocities are indicated by the black dots which are interpolated from measured points from each given gas velocity.

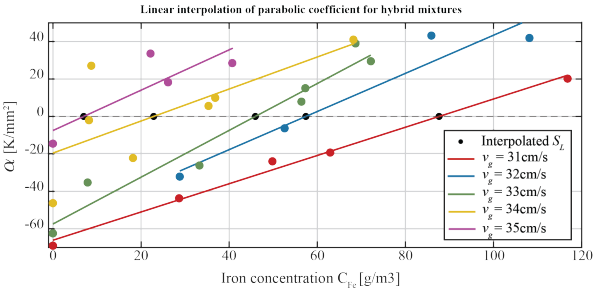

Figure 12: Interpolation of the iron concentration to the adiabatic burning velocity of a hybrid iron-methane-air flame using a stoichiometric methane-air mixture as basis. Each dot indicates a measured parabolic coefficient α.

Figure 13 shows the same data as figure 12 and on the horizontal axis the iron concentration is indicated. The vertical axis displays the gas velocity v_g which corresponds to the burning velocity S_L when the parabolic coefficient equals zero. A clear trend in the burning velocity of hybrid flames as a function of the iron concentration can be seen. In red, the data from Julien et al. [16] is shown for comparison.

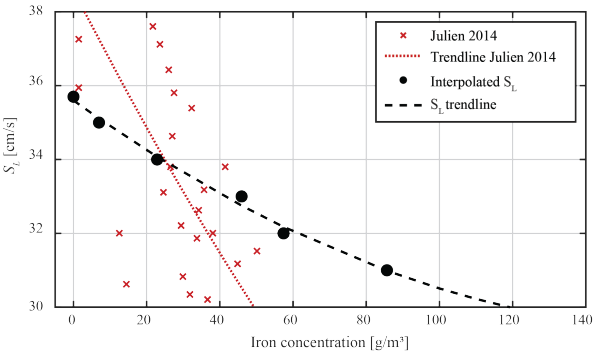

Figure 13: Measured parabolic coefficients and corresponding interpolated burning velocities as function of the iron added to the stoichiometric methane-air mixture. In red the data from Julien et al. [16] is given for comparison.

4 Analysis, validation and discussion

In order to validate the found results for hybrid flames using the HFM, the HHFB should be further investigated. This includes the assumption of a flat, uniform flame, the validation of the dispersion system, and the effect of iron deposition in between the flame and dispersion system. In the following paragraphs, each of these issues is addressed.

Uniformity assumption The principle of the HFM is partially based on the assumption of a uniform flow profile. Hence, a contraction just before the burnerplate is used in the classical HFB. Since the contraction is removed from the burner (illustrated in figure 7), the flow profile of the hybrid burner has to be tested on uniformity. For this validation, PIV measurements were done with the iron particles used as tracers, since they de-

scribe the flow of a iron-methane-air mixture best. Results from cold flow PIV for both the HFB and HHFB are shown in figure 14. Although the boundary region at r = 15 mm seems to be a bit thicker for the HHFB compared to the HFB, the center for both burners show quite a flat flow profile. The spikes and dips shown in figure 14 are caused by the locations where the thermocouples are placed, and thus no flow through the burnerplate is possible. This indicates that the pressure drop of the burnerplate - which is in the range of 2 to 4 Pa for gas velocities between 20 to 40 cm/s respectively - acts sufficiently well as a flow straightener. This statement is also supported by the good agreement of measured values of S_L by the HHFB compared to the HFB in the same infrastructure and literature for methane flames, as readily shown in figure 10. Aside from validation of the flow uniformity, the mixture uniformity also needs to be investigated the future.

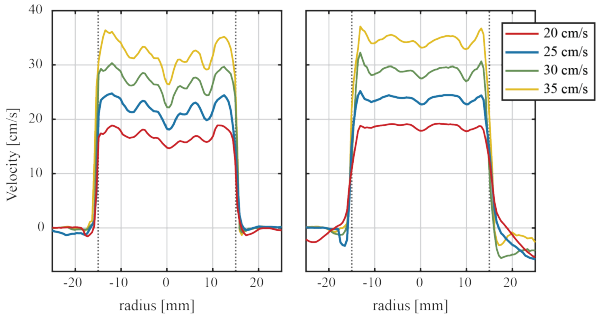

Figure 14: PIV results, from the HFB (left) and the HHFB (right) for varying average gas velocities. Flow profiles were measured about 5 mm above the burner plate.

Dispersion and powder effects The loadcell accuracy was tested by placing a Kern PCB 1000-2 weight scale at the output of the hopper instead of a hose to the burner, causing the particles leaving the dispersion system to fall on the weight scale. A graph of such a measurement is presented in figure 15. Here, it can be seen that the weight gained by the scale is almost equal to the weight lost by the loadcell even though it is mounted on the electromagnetic vibration system.

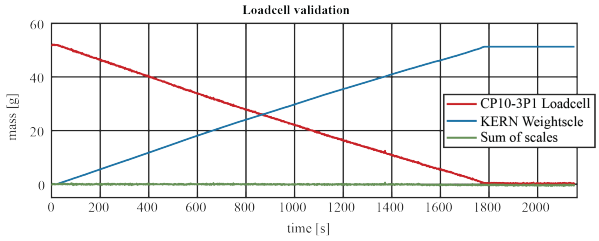

Figure 15: The weight loss of the hopper, measured by the CP10-3P1 loadcell, compared to the mass gain of the KERN weight-scale.

The effect of the vibrations on the particle size distribution was also investigated. The hypothesis was that the vibration of the dispersion system could affect the fed particle size distribution over time, meaning that the size distribution of particles at the start of a session of experiments would be different than the distribution of the fed particles at the end of a session. Analysis of samples taken at the start of a session and at the end indicated that this was not the case.

Flame fluctuations The dispersion system is thus able to control the amount of iron delivered to the flow with reasonable accuracy and stable over time. However, when zooming into the raw data of a measurement, fluctuations of the parabolic coefficient α were detected. These fluctuations could not be redirected to the fluctuations in the loadcell measurements, while these fluctuations were not found in methane-air flames. This means that the fluctuations are induced by the addition of iron to the flame. The issue is illustrated by an example of a measurement given in figure 16. It is hypothesized that there are 2 possible causes for these fluctuations; 1. The loadcell performs well in tracking the average iron mass flow over time (minutes), but fails to detect small fluctuations in the range of seconds. 2. The flame is subjected to the avalanche effect earlier described by Fedoryk [15]. The second issue was for a large part solved by using a beater on the mixing chamber, causing the mixing chamber to vibrate and thus largely restricting particles to accumulate on its walls. Further the data was only taken for time ranges where the both the loadcell data as the parabolic coefficient produced stable values. Such a case is indicated in gray in figure 16.

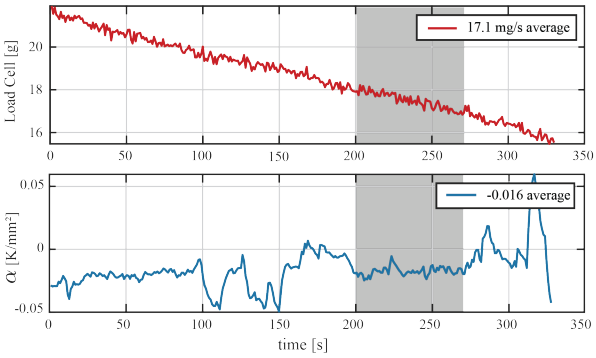

Figure 16: Fluctuations of in α as a consequence of flame fluctuations at a stable mass flow indication from the loadcell. In gray a stable time span is shown which is considered as a valid measurement.

After each session of experiments, the burner was cleaned. It was found that the amount of powder accumulated in the mixing chamber was in the range of 1 to 10% of the powder used. How the accumulation of this powder was build to this point has to be determined in future research. The size distribution of this powder was measured with the Bettersizer S3 Plus, and only minor differences - $\Delta D_{50} \leq 1$ µm - in particle size distribution compared to the initially used particles were found.

Parabolic fit and thermocouple scatter The flame fluctuations as discussed in previous section give rise to uncertainties in the measured temperatures, shown in figure 8. The uncertainties propagate to the corresponding parabolic fit, which also has an uncertainty by itself. The same holds for the determined S_L by the linear fit as described in figure 12. This raises the question about the uncertainties in determining the burning velocity. It was found that the fluctuations in the parabolic coefficient in case of methane flames was significantly lower compared to hybrid flames, indicating that the fluctuations of iron content in the flame are responsible for the largest uncertainties. It is thus advised to further improve the burner and dispersion system by combining the loadcell measurements with LA for the tracking of the iron load fluctuations along with further investigation on the settling of powder on walls.

5 Conclusion and outlook

A new burner in combination with dispersion system is developed for the measurement of hybrid-iron-methane-air burning velocities based on the heat flux method. This burner dispersion combination was tested on flow uniformity and was compared with the classical heat flux burner by methane-air flame measurements, which show good agreement. The in-house developed dispersion system allows for a stable powder feed over time. Aside from small fluctuations in the order of seconds, the burner was able to produce stable hybrid flames. First results of this new burner show a decrease of burning velocity when iron is added to a stoichiometric hybrid flame. Analysis of the experiments indicate that a substantial error can be derived back to the stability of iron mass flow to the flame, and the corresponding fluctuations in flame properties on relatively short time intervals. Future development of the burner using laser attenuation technology can significantly give more insight in these values. This papers was not dedicated to the analysis of a broad set of hybrid flames yet, but does show a proof of concept for a new burner which can be used for such analysis. Extending the possibilities of this burner beyond the metal fuel cycle, all kinds of solid-gas mixtures can be investigated with this new burner. Giving the opportunity for example to also investigate refractory materials.

References

[1] IEA, *World Energy Outlook 2021 - CH 1: Introduction* (2021), https://www.iea.org/reports/world-energy-outlook-2021.

[2] O. Schmidt, S. Melchior, A. Hawkes, and I. Staffell, Projecting the future levelized cost of electricity storage technologies, *Joule* **3**, 81 (2019), ISSN 2542-4351.

[3] N. Conte, How metals prices performed in 2021 (2022), https://elements.visualcapitalist.com/how-metals-prices-performed-in-2021/.

[4] J. Bergthorson, S. Goroshin, M. Soo, P. Julien, J. Palecka, D. Frost, and D. Jarvis, Direct combustion of recyclable metal fuels for zero-carbon heat and power, *Applied Energy* **160**, 368 (2015), ISSN 0306-2619.

[5] S. Sherif, D. Y. Goswami, E. K. Stefanakos, and A. Steinfeld, eds., *Handbook of Hydrogen Energy* (CRC Press, 2014), https://www.routledgehandbooks.com/doi/10.1201/b17226.

[6] I. Glassman, R. A. Yetter, and N. G. Glumac, in *Combustion (Fourth Edition)*, edited by I. Glassman and R. A. Yetter (Academic Press, Burlington, 2008), 703–712, fourth edition ed., ISBN 978-0-12-088573-2.

[7] P. Julien and J. M. Bergthorson, Enabling the metal fuel economy: green recycling of metal fuels, *Sustainable Energy Fuels* **1**, 615 (2017).

[8] L. P. H. D. GOEY, L. M. T. SOMERS, W. M. M. L. BOSCH, and R. M. M. MALLENS, Modeling of the small scale structure of flat burner-stabilized flames, *Combustion Science and Technology* **104**, 387 (1995), arXiv:https://doi.org/10.1080/00102209508907729.

[9] J.-H. Sun, R. Dobashi, and T. Hirano, Structure of flames propagating through metal particle clouds and behavior of particles, *Symposium (International) on Combustion* **27**, 2405 (1998), ISSN 0082-0784.

[10] J.-H. SUN, R. DOBASHI, and T. HIRANO, Combustion behavior of iron particles suspended in air, *Combustion Science and Technology* **150**, 99 (2000), arXiv:https://doi.org/10.1080/00102200008952119.

[11] F.-D. Tang, S. Goroshin, A. Higgins, and J. Lee, Flame propagation and quenching in iron dust clouds, *Proceedings of The Combustion Institute - PROC COMBUST INST* **32**, 1905 (2009).

[12] F.-D. Tang, S. Goroshin, and A. J. Higgins, Modes of particle combustion in iron dust flames, *Proceedings of the Combustion Institute* **33**, 1975 (2011), ISSN 1540-7489.

[13] M. McRae, P. Julien, S. Salvo, S. Goroshin, D. L. Frost, and J. M. Bergthorson, Stabilized, flat iron flames on a hot counterflow burner, *Proceedings of the Combustion Institute* **37**, 3185 (2019), ISSN 1540-7489.

[14] X. Wen, A. Scholtissek, J. van Oijen, J. Bergthorson, and C. Hasse, Numerical modeling of pulverized iron flames in a multidimensional hot counterflow burner, *Combustion and Flame* **248**, 112572 (2023), ISSN 0010-2180.

[15] M. Fedoryk, B. Stelzner, S. Harth, and D. Trimis, Experimental investigation of the laminar burning velocity of iron-air flames in a tube burner, *Applications in Energy and Combustion Science* **13**, 100111 (2023), ISSN 2666-352X.

[16] P. Julien, S. Whiteley, S. Goroshin, M. J. Soo, D. L. Frost, and J. M. Bergthorson, Flame structure and particle-combustion regimes in premixed methane–iron–air suspensions, *Proceedings of the Combustion Institute* **35**, 2431 (2015), ISSN 1540-7489.

[17] L. P. H. de GOEY, A. van MAAREN, and R. M. QUAX, Stabilization of adiabatic premixed laminar flames on a flat flame burner, *Combustion Science and Technology* **92**, 201 (1993).

[18] J. P. Botha and D. B. Spalding, The Laminar Flame Speed of Propane/Air Mixtures with Heat Extraction from the Flame, *Proceedings of the Royal Society of London Series A* **225**, 71 (1954).

[19] A. van Maaren, L. P. H. de Goey, and R. van de Velde, Temperature measurement in flat laminar premixed gas/air flames by laser doppler velocimetry, *International Journal of Energetic Materials and Chemical Propulsion* **3**, 544 (1994), ISSN 2150-766X.

[20] A. Maaren, van, L. Goey, de, and R. Velde, van de, in *Non-intrusive combustion diagnostics, [papers presented at the international symposium on special topics in chemical propulsion], 3rd, Scheveningen, The Netherlands, May 10-14, 1993*, edited by K. Kuo and T. Parr (Begell House Inc., United States, 1994), 544–551, ISBN 1-56700-020-7.

[21] A. V. MAAREN and L. P. H. de GOEY, Laser doppler thermometry in flat flames, *Combustion Science and Technology* **99**, 105 (1994), arXiv:https://doi.org/10.1080/00102209408935427.

[22] K. Bosschaart and L. de Goey, Detailed analysis of the heat flux method for measuring burning velocities, *Combustion and Flame* **132**, 170 (2003), ISSN 0010-2180.

[23] A. Konnov, R. Riemeijer, V. Kornilov, and L. de Goey, 2d effects in laminar premixed flames stabilized on a flat flame burner, *Experimental Thermal and Fluid Science* **47**, 213 (2013), ISSN 0894-1777.

[24] B. Li, J. Lindén, Z. Li, A. Konnov, M. Aldén, and L. de Goey, Accurate measurements of laminar burning velocity using the heat flux method and thermographic phosphor technique, *Proceedings of the Combustion Institute* **33**, 939 (2011), ISSN 1540-7489.

[25] V. A. Alekseev, J. D. Naucler, M. Christensen, E. J. K. Nilsson, E. N. Volkov, L. P. H. de Goey, and A. A. Konnov, Experimental uncertainties of the heat flux method for measuring burning velocities, *Combustion Science and Technology* **188**, 853 (2016), arXiv:https://doi.org/10.1080/00102202.2015.1125348.

[26] S. Goroshin, I. Fomenko, and J. Lee, Burning velocities in fuel-rich aluminum dust clouds, *Symposium (International) on Combustion* **26**, 1961 (1996), ISSN 0082-0784.

[27] P. Julien, M. Soo, S. Goroshin, D. Frost, J. Bergthorson, and N. Glumac, Combustion of aluminum suspensions in hydrocarbon flame products, *J Propuls Power* **30**, 1 (2013).

[28] R. Hermanns, Ph.D. thesis, Mathematics and Computer Science (2007).